Distinct D-Box Motifs in SPD-2 Mediate APC/C^{FZR-1}-Dependent Degradation and Centrosomal Localization in *Caenorhabditis elegans*

Running title: SPD-2 as a substrate of APC/C^{FZR-1}

Rachel N. Yim[1], Paollette A. Rivera[1], Joseph R. DiPanni[1], and Mi Hye Song[1,2]

[1]Department of Biological Sciences, Oakland University, Rochester, MI 48309, USA.

[2]Coresponding Author.

Contact Information: Mi Hye Song (msong2@oakland.edu)

Keywords: Anaphase Promoting Complex, APC/C; FZR-1; *C. elegans*; Centrosome; E3 Ubiquitin Ligase; Proteolysis; SPD-2; ZYG-1; D-box; Degron; Proteasome

Abstract

Centrosome duplication must be tightly controlled to maintain genomic stability. In *Caenorhabditis elegans*, the APC/C and co-activator FZR-1 function as negative regulators of centrosome duplication by targeting specific substrates for proteolytic degradation. While *C. elegans* SAS-5 and ZYG-1 have been identified as substrates of APC/C^{FZR-1}, the mechanism by which APC/C^{FZR-1}-dependent degradation influences centrosome assembly remains elusive. Here, we identified SPD-2, the conserved homolog of human CEP192, as a direct substrate of APC/C^{FZR-1}. We show that loss of APC/C^{FZR-1} increases SPD-2 levels both in the cytoplasm and at centrosomes, and that SPD-2 physically associates with FZR-1 *in vivo*. Functional analyses of canonical D-box motifs demonstrate that all three D-box1, 2, and 3 motifs contribute to SPD-2 degradation, but their functions are distinct. Mutating D-box3 alone rescued *zyg-1* mutant phenotypes by restoring centrosome duplication and embryonic viability through increased centrosomal SPD-2 and ZYG-1. In contrast, mutation of D-box1 or 2 elevated cellular SPD-2 but did not rescue *zyg-1*, with D-box1 mutation further reducing centrosomal SPD-2 and exacerbating duplication defects and lethality in *zyg-1* mutants. Our results reveal a conserved mechanism for APC/C^{FZR-1}-dependent degradation of SPD-2 and show that its degron motifs have dual functions in degradation and centrosomal localization, ensuring robust control of centrosome assembly during *C. elegans* embryogenesis.

Introduction

Centrosomes are the primary microtubule-organizing centers (MTOCs) in animal cells and play crucial roles in spindle assembly, chromosome segregation, and cell fate determination (Nigg and Holland 2018). Their functional capacity depends on the dynamic recruitment of pericentriolar material (PCM) around a centriole core, ensuring that centrosomes are competent for duplication and microtubule nucleation during each cell cycle. Errors in centrosome regulation can cause defective mitotic spindles, genomic instability, and developmental disorders, including microcephaly and cancer (Fernandes-Mariano et al., 2025, Review). Understanding how centrosome assembly and activity are coordinated both in time and space is therefore essential in cell and developmental biology.

A key step in centrosome biogenesis and maturation in *Caenorhabditis elegans* is the recruitment of centrosome components to the site of new centriole formation, a process initiated by the conserved scaffold protein SPD-2 (Kemp et al., 2004; Pelletier et al., 2004) and its upstream factor SAS-7 (Sugioka et al., 2017). SPD-2 localizes to both centrioles and PCM, where it acts upstream of the kinase ZYG-1 (Pelletier et al., 2006; Shimanovskaya et al., 2014) and promotes the recruitment of SPD-5 and γ-tubulin to link PCM assembly with centriole duplication (Kemp et al., 2004). Loss of SPD-2 function significantly impairs centrosome biogenesis, maturation, and microtubule dynamics, underscoring its vital role in centrosome assembly and function (Kemp et al., 2004; Pelletier et al., 2004). Recent structural analyses have further uncovered the modular and intrinsically disordered structure of SPD-2, highlighting its capacity to mediate protein–protein interactions that link centrosome duplication with PCM expansion (Murph et al., 2022). Although SPD-2 is known to be vital for centrosome regulation, its abundance and activity during centrosome assembly in *C. elegans* embryos remain elusive.

Proteolytic regulation by the anaphase-promoting complex/cyclosome (APC/C), an E3 ubiquitin ligase, has emerged as a key mechanism for controlling centrosome activity and maintaining centrosome copy number (Hames et al., 2001; Strnad et al., 2007; Arquint and Nigg 2014; Meghini et al., 2016; Medley et al., 2017; Medley et al., 2021; Tischer et al., 2022; Meghini et al., 2023). In *Drosophila*, APC/C in complex with its co-activator Fizzy-related (Fzr) targets Spd2 for degradation (Meghini et al., 2016). This degradation maintains centrosome asymmetry by limiting Spd2 accumulation at the daughter centrosome, ensuring proper recruitment of PCM and preserving spindle orientation. Without APC/C^{Fzr}-dependent proteolysis, excess Spd2 disrupts

centrosome behavior, impairs microtubule nucleation, and randomizes the division axis (Meghini et al., 2023). These findings demonstrate that proteasome-mediated turnover of conserved centrosome proteins is a crucial mechanism for maintaining centrosome function. Given the conserved role of SPD-2 in centrosome assembly, a similar APC/C-dependent regulation may occur in *C. elegans*. Indeed, SPD-2 functions upstream of ZYG-1 in the centrosome assembly pathway, indicating that precise regulation of SPD-2 levels is critical for promoting centriole duplication and coordinating centrosome maturation (Kemp et al., 2004; Pelletier et al., 2004). Deregulation of SPD-2 levels could therefore have profound consequences for centrosome assembly and function during the cell cycle.

In *C. elegans*, it has been shown that APC/C^{FZR-1} regulates centrosome duplication by promoting degradation of the centrosome protein SAS-5 through its KEN-box motif (Medley et al., 2017) and by modulating centrosomal ZYG-1 levels via D-box motifs (Medley et al., 2021). Loss of FZR-1 or core APC/C subunits elevates SAS-5 and ZYG-1 levels at centrosomes, restoring bipolar spindle formation in hypomorphic *zyg-1* mutants, which reveals that APC/C^{FZR-1} functions at multiple points in the centrosome assembly pathway (Medley et al., 2017; 2021). Furthermore, genetic analyses indicate that APC/C^{FZR-1} targets multiple substrates, including ZYG-1 and SAS-5, as well as other factors that act upstream of ZYG-1. Here, we investigate the hypothesis that APC/C^{FZR-1}-mediated degradation of SPD-2 provides a conserved mechanism to regulate centrosome assembly in *C. elegans*.

Materials and Methods

C. elegans Culture and Genetic Analysis

The *C. elegans* strains used in this study are listed in **Table S1**. All strains were derived from the wild-type Bristol N2 strain (Brenner 1974; Church et al., 1995) and maintained on MYOB plates seeded with *Escherichia coli* OP50 at 16 or 20°C. Some strains were provided by the CGC, which is funded by NIH Office of Research Infrastructure Programs (P40 OD010440). For genetic analysis, individual L4 hermaphrodites were transferred to new plates and allowed to produce progeny for 0-24h, 24-48h, and 48-72h at the indicated temperatures. Progeny were allowed to develop for 18-24 h before counting the number of larvae and dead eggs.

Immunofluorescence and Cytological analysis

Immunofluorescence and confocal microscopy were performed as described (Stubenvoll et al., 2016). The following primary and secondary antibodies were used at 1:3000 dilutions: DM1a

(Millipore Sigma, T9026), α-ZYG-1 (Stubenvoll et al., 2016), α-TBG-1 (Stubenvoll et al., 2016), α-HA (Millipore Sigma, 11867423001, 11583816001; ThermoFisher, 26183-A647), Alexa Fluor 488 and 568 secondary antibodies (ThermoFisher, A11001, A11004, A11006, A11034, A11036). Confocal microscopy was performed using a Nikon Eclipse Ti-U microscope equipped with a Plan Apo 60×1.4 NA lens, a Spinning Disk Confocal (CSU X1), and a Photometrics Evolve 512 camera. MetaMorph software (Molecular Devices, Sunnyvale, CA, USA) was employed for image acquisition and fluorescence intensity quantification, and Adobe Photoshop/Illustrator 2025 for image processing. To quantify fluorescent signals at centrosomes, the average intensity within an 8 or 9-pixel (1 pixel = 0.151 μm) diameter region was recorded for the highest intensity of the focal plane within an area centered on each centrosome. The average intensity within a 25-pixel diameter region outside the embryo was used for background subtraction.

CRISPR/Cas9 Genome Editing

For genome editing, we used the co-CRISPR method described previously (Arribere et al., 2014; Paix et al., 2015). crRNA was designed using the CRISPOR web server (crispor.tefor.net; Concordet and Haeussler, 2018). Animals were microinjected with a mixture of commercially available SpCas9 (IDT, Coralville, IA) and custom-designed oligonucleotides (**Tables S2, S3**) including crRNAs at 0.4–0.8 mg/ml, tracrRNA at 12 mg/ml, and single-stranded DNA oligonucleotides at 25–100 ng/ml. The amount of crRNA was tripled for low-efficiency crRNAs (SPD-2:D-box2). After injection, we screened for *dpy-10(cn64) II/+* rollers in F1 progeny and genotyped F2. The genome editing was confirmed by Sanger sequencing (GeneWiz, South Plainfield, NJ).

Immunoprecipitation (IP) and Immunoblot

IP experiments were performed as described previously (Medley et al., 2023). Embryos were collected from young gravid worms using hypochlorite treatment (1:2:1 ratio of M9 buffer, 5.25% sodium hypochlorite, and 5 M NaOH), frozen in liquid nitrogen, and stored at -80°C until use. Embryos were suspended in lysis buffer [50 mM HEPES, pH 7.4, 2 mM EDTA, pH 8.0, 1 mM $MgCl_2$, 150 mM KCl, 0.5 mM DTT, 0.5% NP-40 (v/v) and 10% glycerol (v/v)] with complete protease inhibitor cocktail (Millipore Sigma) and MG132 (Tocris, Avonmouth, Bristol, UK), milled for 8 minutes (repeat x2) at 30 Hz using a Retsch MM 400 mixer-mill (Verder Scientific, Newtown, PA), then sonicated for 5 minutes in an ultrasonic bath (ThermoFisher). Lysates were spun at 45,000 rpm for 45 minutes using a Sorvall RC M120EX ultracentrifuge (ThermoFisher), then the supernatant was recovered into clean tubes. An equal amount of total protein lysates was used

for each IP. Lysates and α-HA tag magnetic beads (MBL M181-11; Millipore Sigma SAE0197) were incubated with rotation for 1 hour at 4°C and washed (5x 5 minutes) with PBST (PBS + 0.1% Tween-20). IP with beads and input samples were resuspended in 2X Laemmli Sample Buffer (Sigma) and boiled for 5 minutes before fractionating on a 4–12% NuPAGE Bis-Tris gel (ThermoFisher Scientific). Proteins on a gel were transferred to a nitrocellulose membrane and analyzed using the antibodies at 1:3000- 10,000 dilutions: α-SPD-2 (Song et al., 2008), α-TBG-1 (Stubenvoll et al., 2016), DM1a (Sigma T9026), α-Ollas (ThermoFisher MA5-16125), α-HA (Millipore Sigma 11867423001, 11583816001), IRDye secondary antibodies (LI-COR Biosciences). Blots were imaged with the Odyssey M scanner (LI-COR Biosciences) and analyzed using Image Studio software (LI-COR Biosciences).

Statistical analysis

Statistics were produced using R statistical software and presented as average ± standard deviation (SD). Dotplots were generated using the R 'beeswarm' package. In the dotplots, box ranges from the first through the third quartile of the data. The thick bar indicates the median. Solid grey line extends 1.5 times the inter-quartile range or to the minimum and maximum data point. All P-values were calculated using two-tailed t-tests: ^{ns} $p>0.05$, * $p<0.05$, ** $p<0.01$, *** $p<0.001$.

Results and Discussion

Loss of FZR-1 stabilizes cellular SPD-2

If APC/C^{FZR-1} directly targets SPD-2 for proteasomal degradation, then inhibiting APC/C^{FZR-1} should block SPD-2 degradation, thereby hyper-stabilizing SPD-2 and elevating its total cellular levels. First, we examined whether loss of APC/C^{FZR-1} affected SPD-2 abundance by quantitative Western blot analysis using anti-SPD-2 (Song et al., 2008) and protein lysates extracted from *fzr-1(bs31)* mutant (Medley et al., 2017) and wild-type (WT) embryos (**Figure 1A**).

Our quantification data revealed that SPD-2 levels in *fzr-1(bs31)* mutant embryos are significantly higher (1.89±0.71-fold, $p<0.001$, n=27) than those in WT controls (1.00±0.0-fold, n=24), whereas *zyg-1* mutant embryos show no significant changes (0.94±0.16-fold, n=10). In contrast, TBG-1 levels seem unaffected in both mutants. These findings indicate that loss of APC/C^{FZR-1} leads to increased overall cellular SPD-2 levels, likely due to hyper-stabilization. We observed a similar

trend in *mat-3(or180)* for the core APC8/CDC23 subunit (Golden et al., 2000) and *emb-1(hc57)* mutants for the APC16 in the *C. elegans* APC/C complex (Shakes et al., 2011) (**Figure S1A**).

Then, increased levels of cellular SPD-2 in the embryo can influence the amount of SPD-2 recruited to centrosomes. To evaluate SPD-2 levels at centrosomes, we stained embryos with anti-HA and measured the fluorescence intensity of the SPD-2::2xHA signal at centrosomes (Medley et al., 2023). As SPD-2 localizes to both centrioles and PCM, we measured total centrosomal (both centriolar and PCM) and only centriolar SPD-2 signals (**Figure 1B**). Quantitative immunofluorescence (IF) using SPD-2 tagged with 2xHA (SPD-2::2xHA; Medley et al., 2023) revealed that during the first mitosis, *fzr-1(bs31)* mutant embryos exhibit increased levels of **t**otal centrosomal SPD-2::2xHA (1.50±0.44-fold, n=92 at metaphase; 1.42±0.37-fold, n=39 at anaphase) compared to WT controls (1.00±0.36-fold, n=47 at metaphase; 1.00±0.31-fold, n=33 at anaphase). A similar increase was also observed in *mat-3(or180)* for the core APC8/CDC23 subunit (Golden et al., 2000; **Figure S1B**). We also observed a similar trend for the centriolar SPD-2 levels. The *fzr-1(bs31)* mutant embryo exhibits increased levels of centriolar SPD-2::2xHA (1.50±0.46-fold, n=98 at metaphase; 1.36±0.44-fold, n=39 at anaphase) compared to WT controls (1.00±0.33-fold, n=48 at metaphase; 1.00±0.30-fold, n=36 at anaphase; **Figure S1C**). Since our prior study showed that *fzr-1(bs31)* mutant embryos contain elevated centrosomal ZYG-1 levels (Medley et al., 2021), we also measured ZYG-1 levels by co-staining embryos with anti-HA and anti-ZYG-1 (Stubenvoll et al., 2016). The *fzr-1(bs31)* mutant embryo shows increased levels of centrosomal ZYG-1 (1.35±0.35-fold, n=80 at metaphase; 1.55±0.49-fold, n=31 at anaphase) compared to WT controls (1.00±0.26-fold, n=31 at metaphase; 1.00±0.23-fold, n=32 at anaphase), consistent with prior observations (Medley et al., 2021; **Figure 1B**). Our data show that loss of APC/C^{FZR-1} leads to a significant increase in both cellular and centrosomal levels of SPD-2, supporting a model in which APC/C^{FZR-1}-dependent proteolysis regulates SPD-2 abundance during *C. elegans* embryogenesis. Quantitative Western blot analysis showed that cellular SPD-2 levels are elevated by loss of APC/C^{FZR-1}, and the corresponding increase at centrosomes is likely a direct consequence of this increase in cellular SPD-2.

Furthermore, our immunoprecipitation (IP) assays using embryonic lysates indicate a physical interaction between SPD-2 and FZR-1 *in vivo* (**Figure 1C**). We detected SPD-2::2xHA and Ollas::FZR-1 in the pull-down using embryonic lysates expressing SPD-2::2xHA (Medley et al., 2023) and Ollas::FZR-1 (Medley et al., 2021). Together, these results support our hypothesis that APC/C^{FZR-1} directly targets SPD-2 for proteasomal degradation. Our results support our model, in

which the APC/C and its co-activator FZR-1 (APC/C^{FZR-1}) regulate SPD-2 abundance in *C. elegans* embryos.

SPD-2 Contains Five Putative D-box Motifs

The E3 ubiquitin ligase APC/C^{FZR-1} targets specific substrates through the coactivator FZR-1, which directly recognizes conserved motifs, mainly the destruction (D)-box and KEN-box, within the substrate (Glotzer et al., 1991; Pfleger and Kirschner, 2000). Our *in-silico* analysis identified five putative D-box motifs (RxxL), but no KEN-box, within the *C. elegans* SPD-2 (**Figure 2A**). In SPD-2, D-box1 is located within the coiled-coil (CC3: aa291-322) domain, D-box2 within the Aspm-SPD-2-Hydin (ASH) domain, D-box3 between Ig-like and PDZ domains, and both D-box4 and D-box5 within the PDZ domain (Murph et al., 2022). The sequence alignments show that D-box4 is the only conserved motif among closely related nematodes (**Figure 2B**). We also noted a pattern of sequence conservation within the D-box motifs (**Figure 2B**).

We first asked whether APC/C^{FZR-1} targets SPD-2 by directly recognizing the canonical D-box degron. To determine if any of the five putative D-box motifs function as degrons *in vivo* by mediating FZR-1 and SPD-2 interaction, we used CRISPR/Cas9 genome editing to generate degron mutants by replacing two critical residues within each D-box motif (RxxL) with alanine (AxxA) at their endogenous loci. Viable degron mutants were successfully produced for D-box1, D-box2, and D-box3, each with two-alanine substitutions, referred to as the SPD-2:DB1(2A), SPD-2:DB2(2A), and SPD-2:DB3(2A) mutations (**Table 1**). However, homozygous 2A mutations in D-box4 and D-box5 were lethal, indicating that these conserved motifs are essential for embryonic survival. Notably, a genome-wide genetic screen identified the *spd-2(oj29: R710Q)* mutation, which alters the first Arg (R) residue of D-box4 (710-**R**TRL-713) and causes centrosome duplication failure and embryonic lethality (**Figure 2A**, Kemp et al., 2004). As a result, we were unable to evaluate the functional roles of the D-box4 and D-box5 degron motifs *in vivo*. Due to this limitation, we focused our analysis on D-boxes 1, 2, and 3 (DB1, 2, and 3) by using viable degron mutants to assess their functional effects in this study.

Mutating the D-box leads to elevated overall cellular SPD-2 levels

If APC/C^{FZR-1} targets SPD-2 by directly recognizing its D-box motif, mutating the D-box degron should prevent APC/C^{FZR-1} from binding to SPD-2, thereby protecting SPD-2 from degradation and increasing its levels. To assess how the D-box motif affects overall SPD-2 levels, we conducted quantitative Western blot analysis using protein lysates from each degron mutant embryo expressing SPD-2::2xHA (Medley et al., 2023; **Figure 2C**). Our results indicated that

SPD-2 levels in all three D-box mutant embryos are significantly higher (DB1: 1.72±0.43-fold, n=24; DB2: 2.10±0.57-fold, n=17; DB3: 2.09±0.43-fold, n=11, $p<0.001$) compared to wild-type embryos (1.00±0.0-fold, n=17). In contrast, TBG-1 levels remain unaffected in degron mutants. These findings suggest that mutating the D-box motifs renders SPD-2 resistant to degradation, supporting the idea that the three D-box motifs (DB1, DB2, and DB3) in SPD-2 function as degrons recognized by APC/C^{FZR-1}. Inhibiting this recognition blocks SPD-2 degradation, leading to its accumulation and mimicking SPD-2 overexpression.

Centrosomal SPD-2 levels are increased only in the DB3 mutants but are significantly decreased in the DB1 mutants

Our quantitative Western blot analysis shows that the SPD-2 degron mutation stabilizes SPD-2 protein by inhibiting proteasomal degradation, leading to higher overall SPD-2 levels in the embryo. To determine whether this increase impacts SPD-2 activity at centrosomes, we examined how each degron mutation affects centrosomal SPD-2 levels. Using quantitative immunofluorescence (IF), we measured total centrosomal SPD-2 levels during the first mitosis in embryos expressing SPD-2::2xHA stained with antibodies for HA tag and tubulin (Medley et al., 2021; **Figure 2D**).

The SPD-2:DB3(2A) mutation led to elevated centrosomal SPD-2 levels (1.35±0.43-fold, $p<0.001$, n=45 at metaphase; 1.32±0.42-fold, $p<0.0001$, n=34 at anaphase) compared to WT controls (1.00±0.33-fold, n=60 at metaphase; 1.00±0.27-fold, n=38 at anaphase). These results suggest that the SPD-2:DB3(2A) mutation retains its normal ability of centrosomal SPD-2 loading. Therefore, higher cellular SPD-2 levels lead to increased SPD-2 at centrosomes. In contrast, the SPD-2:DB1(2A) mutation caused a significant decrease in centrosomal SPD-2 (0.59±0.20-fold, $p<0.001$, n=28 at metaphase; 0.66±0.26-fold, $p<0.001$, n=10 at anaphase) compared to controls. This dramatic reduction of centrosomal SPD-2 in the DB1(2A) mutant indicates that the D-box1 motif is critical for SPD-2 localization to centrosomes, implicating its dual role as both a degron and a key site for subcellular localization. Meanwhile, the DB2(2A) mutation caused no significant changes in centrosomal SPD-2 (1.06±0.40-fold, $p=0.55$, n=21 at metaphase; 1.12±0.68-fold, $p=0.40$, n=6 at anaphase) although the DB2(2A) mutation increases overall SPD-2 levels, indicating that the SPD-2:DB2(2A) mutation partially impairs SPD-2 localization to centrosomes. These degron mutants also exhibited consistent trends in centriolar SPD-2 levels (**Figure S2A**). The SPD-2:DB3(2A) mutant embryo contains higher levels (1.23±0.29-fold, n=31 at metaphase; 1.13±0.22-fold, n=35 at anaphase), while the DB1(2A) mutants have reduced levels (0.57±0.18-fold, n=28 at metaphase; 0.63±0.17-fold, n=10 at anaphase) and the DB2(2A) embryos show no

change (1.07±0.46-fold, n=21 at metaphase; 0.98±0.2-fold, n=8 at anaphase), compared to WT controls (1.00±0.33-fold, n=56 at metaphase; 1.00±0.23-fold, n=27 at anaphase).

Additionally, to investigate how SPD-2 degron mutations affect ZYG-1 recruitment, we also measured centrosomal ZYG-1 levels in degron mutant embryos stained with anti-ZYG-1 and anti-tubulin (Stubenvoll et al., 2016; **Figure 2E**). The SPD-2:DB3(2A) mutant embryos displayed higher centrosomal ZYG-1 (1.14±0.29-fold, $p<0.01$, n=57 at metaphase; 1.21±0.21-fold, $p<0.001$, n=31 at anaphase) compared to WT controls (1.00±0.28-fold, n=72 at metaphase; 1.00±0.25-fold, n=45 at anaphase). In contrast, DB1(2A) mutants showed a marked reduction in centrosomal ZYG-1 (0.50±0.13-fold, $p<0.001$, n=24 at metaphase; 0.45±0.13-fold, $p<0.001$, n=19 at anaphase), whereas DB2(2A) mutants exhibited a slight decrease with no significant difference (0.84±0.10-fold, $p=0.07$, n=10 at metaphase; 0.88±0.09-fold, $p=0.09$, n=14 at anaphase). These results are consistent with the observed patterns of centrosomal SPD-2 levels across the degron mutants (**Figure 2D**).

The DB3(2A) mutation leads to *zyg-1* suppression

Next, we investigated how specific degron mutations impacted SPD-2 activity in regulating centrosome assembly, using the hypomorphic *zyg-1(it25)* genetic background. The *zyg-1(it25)* allele carries a temperature-sensitive (ts) mutation (P442L) in the cryptic polo-box (CPB) domain, which is critical for centrosomal recruitment of ZYG-1 (Kemphues et al., 1988; Shimanovskaya et al., 2014). At the restrictive temperature 24°C, *zyg-1(it25*) mutant embryos fail to duplicate centrosomes during the first mitosis, leading to monopolar spindle formation in the second mitosis and resulting in 100% embryonic lethality (O'Connell et al., 2001). In the molecular hierarchy, SPD-2 functions upstream of ZYG-1 and is required for ZYG-1 loading to centrioles before procentriole formation (Pelletier et al., 2006).

If APC/C^{FZR-1} targets SPD-2 for degradation via its D-box degron, mutating the D-box motif should block APC/C^{FZR-1} binding, thereby stabilizing SPD-2. Then, hyper-stabilized SPD-2, resembling overexpression, could compensate for the reduced ZYG-1 activity in *zyg-1(it25)* mutants. To determine whether any SPD-2 D-box mutation could rescue *zyg-1(it25)* phenotypes, we introduced each mutation into the *zyg-1(it25)* background by genetic crossing and examined their effects on embryonic survival and centrosome duplication. Consistent with our hypothesis, the SPD-2:DB3(2A) mutation restored embryonic viability (35±16% vs 18±14%, $p<0.001$; **Table 1, S4, Figure 3A**) and bipolar spindle formation (61±15% vs 34±22%, $p<0.01$; **Figure 3B**) in *zyg-1* mutants at the semi-restrictive temperature (22.5°C). This rescue effect was more potent at

22.5°C (35±16%) than at a more restrictive temperature condition 23°C (5±4%; **Table 1**), suggesting that the SPD-2:DB3(2A) mutation depends on residual ZYG-1 activity for suppression. However, suppression of *zyg-1* by the SPD-2:DB3(2A) mutation appeared significantly weaker than that observed with the *fzr-1* mutation (100% bipolar spindles and embryonic viability; **Figure 3B, Table 1**; Medley et al., 2021).

However, the SPD-2:DB1(2A) mutation markedly decreased embryonic viability (0.5±0.9% vs 18±14%, $p<0.001$; **Figure 3A, Table 1**) and bipolar spindles (1.2±2.2% vs 34±22%, $p<0.001$; **Figure 3B**) in *zyg-1(it25)* mutants, whereas the SPD-2:DB1(2A) mutant alone remained largely viable (99.2±1.1%; **Table 1**). These results indicate that *zyg-1(it25)* provides a sensitized genetic background in which SPD-2:DB1(2A) causes near-complete lethality, demonstrating a strong synthetic effect. Consistently, although *spd-2* and *zyg-1* mutations are individually recessive, *spd-2/+; zyg-1/+* double heterozygotes exhibit ~75% embryonic lethality (Song et al., 2011). DB1(2A) mutant embryos have centrosomal SPD-2 levels at 59% of those in wild-type embryos, similar to those in *spd-2* heterozygotes (*spd-2*/+), despite exhibiting elevated total cellular SPD-2 levels. Thus, D-box1 appears to regulate centrosomal loading of SPD-2 independently of its degron function. Although 59% of centrosomal SPD-2 is sufficient to support ZYG-1 loading and normal centrosome duplication in a wild-type background, combining the DB1(2A) mutation with homozygous *zyg-1(it25)* severely disrupts centrosome duplication and mitosis, leading to near-complete embryonic lethality at the semi-restrictive temperature (22.5°C), where *zyg-1(it25)* alone causes ~80% lethality (**Table 1**). These findings suggest that the D-box1 motif promotes proper SPD-2 centrosomal localization and may facilitate its interaction with ZYG-1. D-box1 resides within the CC3 domain (**Figure 2A**), and the DB1(2A) mutation consists of two alanine substitutions (R298A and L301A). Since coiled-coil domains are known to mediate protein–protein interactions (Murph et al., 2022), these substitutions likely impair the ability of SPD-2 to interact with binding partners necessary for centrosome function.

Meanwhile, the SPD-2:DB2(2A) mutation had a minimal negative impact on embryonic viability (14.4±17.6% vs 18±14%, $p=0.36$; **Table 1, Figure 3A**) and bipolar spindle formation (30.2±18.5% vs 34±22%, $p=0.55$; **Figure 3B**) in *zyg-1(it25)* mutants. Like DB1(2A), the DB2(2A) mutation increased overall SPD-2 levels but did not enhance its centrosomal activity, suggesting a partial defect in SPD-2 loading, though much milder than DB2(2A). Since it resides within the ASH domain, which is known to target SPD-2 to centrosomes (Murph et al., 2022), this may partly

explain the modest yet negative impact of the DB2(2A) mutation on embryonic lethality, unlike its effect on SPD-2 stability.

The DB3(2A) mutation leads to increased centrosomal ZYG-1 levels in *zyg-1(it25)* mutants

In *zyg-1(it25)* embryos, centrosomal ZYG-1 is reduced to ~40% of WT controls (Medley et al., 2017), impairing the recruitment of SAS-5 and SAS-6, which are required for subsequent SAS-4 loading to centrosomes (Pelletier et al., 2006). Since SPD-2 acts upstream of ZYG-1 and promotes centrosomal recruitment of ZYG-1 (Pelletier et al., 2006), the observed suppression of *zyg-1* mutant phenotypes is probably due to increased centrosomal ZYG-1 levels driven by SPD-2 accumulation. Consequently, increased levels of centrosomal ZYG-1 may restore recruitment of downstream factors, rendering centrosomes competent to assemble new centrioles in *zyg-1(it25)* mutants.

To assess how the SPD-2 degron mutation influenced ZYG-1 recruitment in *zyg-1(it25)* mutants, we measured centrosomal ZYG-1 levels in *zyg-1(it25)* embryos carrying each degron mutation (**Figure 3C**). As expected, the SPD-2:DB3(2A) mutation increased centrosomal ZYG-1 levels (1.15±0.22-fold, $p<0.0001$, n=52 at metaphase; 1.20±0.29-fold, $p<0.0001$, n=43 at anaphase) compared to *zyg-1(it25)* controls (1.00±0.14-fold, n=44 at metaphase; 1.00±0.15-fold, n=33 at anaphase). Conversely, the DB1(2A) mutation significantly reduced centrosomal ZYG-1 (0.53±0.14-fold, $p<0.001$, n=24 at metaphase; 0.31±0.06-fold, $p<0.001$, n=6 at anaphase), while DB2(2A) mutants showed a slight decrease (0.92±0.18-fold, $p=0.466$, n=12 at metaphase; 0.91±0.29-fold, $p=0.02$, n=10 at anaphase).

These results align with the patterns of centrosomal SPD-2 levels across each degron mutant combined with *zyg-1(it25)* (**Figure S3A**). The SPD-2:DB3(2A) mutation caused higher centrosomal SPD-2 levels (1.22±0.35-fold, $p<0.001$, n=66 at metaphase; 1.25±0.28-fold, $p<0.001$, n=69 at anaphase), while DB1(2A) resulted in a dramatic decrease (0.74±0.25-fold, $p<0.001$, n=22 at metaphase; 0.74±0.29-fold, $p<0.001$, n=33 at anaphase), and DB2(2A) showed a slight reduction (0.86±0.22-fold, $p<0.01$, n=42 at metaphase; 1.03±0.24-fold, $p=0.68$, n=13 at anaphase), relative to *zyg-1(it25)* controls (1.00±0.29-fold, n=76 at metaphase; 1.00±0.19-fold, n=30 at anaphase). Lastly, we observed lower levels of centrosomal SPD-2 compared to the *fzr-1(bs31)* mutation, both in *zyg-1(it25)* backgrounds (1.25±0.28-fold, n=69 vs 2.59±0.89-fold, n=14, $p<0.001$; **Figure S3B**), which is consistent with the weaker suppression of *zyg-1* by the SPD-2:DB3(2A) mutation relative to the *fzr-1* mutation.

SPD-2:DB3(2A) mutant embryos exhibit increased cellular SPD-2 levels, resulting in higher centrosomal levels of SPD-2 and ZYG-1. However, the SPD-2:DB3(2A) mutation alone produces a much weaker rescue of embryonic viability (1.25±0.28% vs 100%, **Table 1**) and bipolar spindle formation (60±15% vs 100±0%, **Figure 2B**) in *zyg-1(it25)* mutants, compared to the *fzr-1* mutation (**Figure S3B, Table 1**). Similar results were observed in our previous work, where ZYG-1 or SAS-5 degron mutations led to *zyg-1* suppression that was less effective than the *fzr-1* mutation (Medley et al., 2017; 2021). Multiple factors may explain the lower impact of the *zyg-1* suppression by SPD-2:DB3(2A) single mutation. D-box4 and 5 (DB4 and DB5) were not tested for functional roles as degrons because of their homozygous lethality, as DB4 and DB5 could be more critical degrons. In this study, we did not perform *in vitro* tests for DB4 and DB5 as potential functional degrons. Therefore, the *zyg-1* suppression by the SPD-2:DB3(2A) mutation alone does not reflect the full impact of loss of APC/C^{FZR-1} because SPD-2 degradation might not be blocked entirely. Therefore, we observe a partial rescue effect in *zyg-1* mutants, which is less pronounced than that of the *fzr-1* mutation.

At any event, our findings show that the SPD-2:DB3(2A) mutation elevates centrosomal ZYG-1, thereby enhancing the recruitment of downstream factors and restoring centrosome duplication and embryonic viability in *zyg-1* mutants. This suggests a possible mechanism by which SPD-2:DB3(2A) suppresses the *zyg-1* phenotype.

SPD-2:DB1(2A) mutant embryos exhibit abnormal cell division

During our genetic analysis at 25°C, we observed a low but significant rate of embryonic lethality in the SPD-2::DB1(2A) mutants, and this lethality was further exacerbated in the 2xHA-tagged SPD-2:DB1(2A) mutant (1.2% vs 4.8% lethality; **Table 1**). To determine the cause of embryonic lethality, we examined SPD-2:DB1(2A):2xHA mutant embryos stained for centrosomes, microtubules, and DNA (**Figure 4**). At 25°C, DB1(2A) mutant embryos display abnormal cell division phenotypes. Consistent with reduced levels of SPD-2 and ZYG-1 at centrosomes (**Figure 2D-E**), these embryos show tiny centrosomes and often highly asymmetric centrosome sizes during the first mitotic metaphase. They also exhibit abnormal patterns in DNA segregation, cell division timing, and mitotic division patterns compared to the WT control, although at a low frequency (<5%, n>100). These cell division defects likely account for embryonic lethality and further confirm that the D-box1 motif functions not only as a degron motif but also plays a critical role in SPD-2 localization and its centrosomal activity, promoting ZYG-1 recruitment. Thus, our study uncovered new key sites critical for SPD-2 activity in centrosome assembly.

In this study, we identified *C. elegans* SPD-2 as a direct substrate of APC/C^{FZR-1} and uncovered a regulatory network that links protein degradation, centrosomal localization, and interactions with other partners. We demonstrate that SPD-2 physically interacts with FZR-1 *in vivo*, and that loss of APC/C^{FZR-1} results in elevated levels of both cellular and centrosomal SPD-2. These results expand the repertoire of APC/C^{FZR-1} substrates beyond SAS-5 and ZYG-1 (Medley et al., 2017; 2021), underscoring the crucial role of APC/C^{FZR-1} in regulating centrosome assembly during *C. elegans* embryogenesis. Importantly, our results also suggest that APC/C^{FZR-1} may target additional centrosome factors, with SAS-7 (Sugioka et al., 2017) as a strong candidate for future research.

Our degron motif analysis reveals both canonical and noncanonical functions. While all three D-box mutations (DB1, DB2, DB3) stabilized SPD-2, only the DB3 mutation restores centrosome duplication and embryonic viability in *zyg-1* mutants. Our results also uncovered that DB1 and DB2 have functions beyond their roles as degron motifs. The DB1 motif is required for efficient localization of SPD-2 to centrosomes and possibly for its interaction with ZYG-1, and DB1 mutants exhibit reduced centrosomal SPD-2 and ZYG-1 levels, leading to monopolar spindle formation and increased embryonic lethality in *zyg-1* mutants. This suggests that DB1 may be required for both centrosomal stabilization and targeting of SPD-2. By contrast, DB2 mutation increased total SPD-2 levels but did not alter centrosomal pools or rescue *zyg-1* phenotypes. These results highlight functional diversification of degron motifs, with DB1 and DB2 contributing to both degradation and centrosomal activity.

Our findings provide broader evolutionary significance. SPD-2/CEP192 is a highly conserved key regulator of centrosome assembly in metazoans (Kemp et al., 2004; Pelletier et al., 2004; Zhu et al., 2008). By demonstrating how degron motifs link proteolytic degradation with centrosomal localization, our study reveals how centrosome proteins are controlled both quantitatively and qualitatively. Because dysregulation of centrosome factors is closely associated with genomic instability and tumorigenesis in higher eukaryotes (Nigg and Holland, 2018), understanding degron-dependent regulation of SPD-2 in *C. elegans* and *Drosophila* (Meghini et al., 2016; 2023) provides an evolutionary framework for investigating analogous mechanisms in human cells. Future work should explore how APC/C^{FZR-1} contributes to centrosome assembly and MTOC function, with implications for human health and cancer biology.

Table 1. Genetic Analysis

Strain	°C	% Embryonic viability (ave ± sd)	n (progeny)
wild-type (N2)	25	99.8 ± 0.3	2214
SPD-2$^{DB1(2A)}$		98.8 ± 1.0*	2298
SPD-2$^{DB2(2A)}$		100.0 ± 0.0	1224
SPD-2$^{DB3(2A)}$		99.9± 0.2	2313
SPD-2::2xHA	25	99.2 ± 0.7	2322
SPD-2$^{DB1(2A)}$::2xHA		95.2± 2.7**	2124
SPD-2$^{DB2(2A)}$::2xHA		99.4 ± 0.5	2431
SPD-2$^{DB3(2A)}$::2xHA		100.0± 0.0**	1648
zyg-1(it25)	22.5	18.2 ± 14.4	6053
SPD-2$^{DB1(2A)}$; zyg-1(it25)		0.5 ± 0.9***	6249
SPD-2$^{DB2(2A)}$; zyg-1(it25)		14.4 ± 17.6	4913
SPD-2$^{DB3(2A)}$; zyg-1(it25)		34.5 ± 15.9***	6285
zyg-1(it25) fzr-1(bs31)		100.0± 0.0***	1848
zyg-1(it25)	23	0.0 ± 1.0	1163
SPD-2$^{DB1(2A)}$; zyg-1(it25)		0.0 ± 0.0	859
SPD-2$^{DB2(2A)}$; zyg-1(it25)		0.0 ± 0.6	710
SPD-2$^{DB3(2A)}$; zyg-1(it25)		5.0 ± 4.3***	1095

*** $p<0.001$, ** $p<0.01$, * $p<0.05$, compared to controls

Acknowledgements

We thank former and current members of the Song lab for their technical support. We especially thank WormBase and the *Caenorhabditis* Genetics Center (CGC). WormBase is supported by grant U24HG002223 from the National Human Genome Research Institute at the US National Institutes of Health, the UK Medical Research Council, and the UK Biotechnology and Biological Sciences Research Council. The CGC (St. Paul, MN) is funded by the National Institutes of Health Office of Research Infrastructure Programs (P40 OD010440).

Competing Interests

No competing interests declared.

Author Contributions

M.H.S. designed the experiments, wrote the manuscript, and performed quantifications of confocal imaging and protein levels from western blots. R.N.Y., P.R., J.D., and M.H.S. performed experiments and provided data.

Funding

This work was supported by a grant [7R15GM11016-02 to M.H.S.] from the National Institute of General Medical Sciences. The funders had no role in study design, data collection and analysis, decision to publish, or manuscript preparation.

References

Arquint, C., and E. A. Nigg, 2014 STIL microcephaly mutations interfere with APC/C-mediated degradation and cause centriole amplification. Curr Biol 24: 351-360.

Arribere, J.A., R.T. Bell, B.X. Fu, K.L. Artiles, P.S. Hartman, and A.Z. Fire. (2014).Efficient marker-free recovery of custom genetic modifications with CRISPR/Cas9 in Caenorhabditis elegans. Genetics. 198:837-846.

Brenner, S. 1974 The genetics of Caenorhabditis elegans. Genetics. 77:71-94.
Church, D.L., K.L. Guan, and E.J. Lambie, 1995 Three genes of the MAP kinase cascade, mek-2, mpk-1/sur-1 and let-60 ras, are required for meiotic cell cycle progression in Caenorhabditis elegans. Development. 121:2525-2535.

Fernandes-Mariano, C., J. N. Bugalhao, D. Santos and M. Bettencourt-Dias, 2025 Centrosome biogenesis and maintenance in homeostasis and disease. Curr Opin Cell Biol 94: 102485.

Garcia-Higuera, I., E. Manchado, P. Dubus, M. Canamero, J. Mendez et al., 2008 Genomic stability and tumour suppression by the APC/C cofactor Cdh1. Nat Cell Biol 10: 802-811.

Glotzer, M., A. W. Murray and M. W. Kirschner, 1991 Cyclin is degraded by the ubiquitin pathway. Nature 349: 132-138.

Golden, A., P. L. Sadler, M. R. Wallenfang, J. M. Schumacher, D. R. Hamill et al., 2000 Metaphase to anaphase (mat) transition-defective mutants in Caenorhabditis elegans. J Cell Biol 151: 1469-1482.

Hames, R. S., S. L. Wattam, H. Yamano, R. Bacchieri and A. M. Fry, 2001 APC/C-mediated destruction of the centrosomal kinase Nek2A occurs in early mitosis and depends upon a cyclin A-type D-box. EMBO J 20: 7117-7127.

Hu, L., A. Wainman, A. Andreeva, M. Apizi, I. Alvarez-Rodrigo et al., 2025 The conserved Spd-2/CEP192 domain adopts a unique protein fold to promote centrosome scaffold assembly. Sci Adv 11: eadr5744.

Kemp, C. A., K. R. Kopish, P. Zipperlen, J. Ahringer and K. F. O'Connell, 2004 Centrosome maturation and duplication in C. elegans require the coiled-coil protein SPD-2. Dev Cell 6: 511-523.

Kemphues, K. J., M. Kusch and N. Wolf, 1988 Maternal-effect lethal mutations on linkage group II of Caenorhabditis elegans. Genetics 120: 977-986.

Medley, J. C., L. E. DeMeyer, M. M. Kabara and M. H. Song, 2017 APC/CFZR-1 Controls SAS-5 Levels To Regulate Centrosome Duplication in Caenorhabditis elegans. G3 Genes|Genomes|Genetics 7: 3937-3946.

Medley, J. C., J. R. DiPanni, L. Schira, B. M. Shaffou, B. M. Sebou et al., 2021 APC/CFZR-1 regulates centrosomal ZYG-1 to limit centrosome number. J Cell Sci 134.
Medley, J. C., R. N. Yim, J. DiPanni, B. Sebou, B. Shaffou et al., 2023 Site-specific phosphorylation of ZYG-1 regulates ZYG-1 stability and centrosome number. iScience 26: 108410.

Meghini, F., T. Martins, X. Tait, K. Fujimitsu, H. Yamano et al., 2016 Targeting of Fzr/Cdh1 for timely activation of the APC/C at the centrosome during mitotic exit. Nat Commun 7: 12607.

Meghini, F., T. Martins, Q. Zhang, N. Loyer, M. Trickey et al., 2023 APC/C-dependent degradation of Spd2 regulates centrosome asymmetry in Drosophila neural stem cells. EMBO Rep 24: e55607.

Murph, M., S. Singh and M. Schvarzstein, 2022 A combined in silico and in vivo approach to the structure-function annotation of SPD-2 provides mechanistic insight into its functional diversity. Cell Cycle 21: 1958-1979.

Nakayama, K. I., and K. Nakayama, 2006 Ubiquitin ligases: cell-cycle control and cancer. Nat Rev Cancer 6: 369-381.

Nigg, E. A., and A. J. Holland, 2018 Once and only once: mechanisms of centriole duplication and their deregulation in disease. Nat Rev Mol Cell Biol 19: 297-312.

O'Connell, K. F., C. Caron, K. R. Kopish, D. D. Hurd, K. J. Kemphues et al., 2001 The C. elegans zyg-1 gene encodes a regulator of centrosome duplication with distinct maternal and paternal roles in the embryo. Cell 105: 547-558.

Paix, A., A. Folkmann, D. Rasoloson, and G. Seydoux.(2015). High Efficiency, Homology-Directed Genome Editing in Caenorhabditis elegans Using CRISPR-Cas9 Ribonucleoprotein Complexes. Genetics. 201:47-54.

Pelletier, L., Ozlu, N., Hannak E., Cowan C., Habermann B., Ruer M., Muller-Reichert T., Hyman AA, 2004 The Caenorhabditis elegans centrosomal protein SPD-2 is required for both pericentriolar material recruitment and centriole duplication. Current Biology 25: 863-73.

Pelletier, L., E. O'Toole, A. Schwager, A. A. Hyman and T. Muller-Reichert, 2006 Centriole assembly in Caenorhabditis elegans. Nature 444: 619-623.

Pfleger, C. M., and M. W. Kirschner, 2000 The KEN box: an APC recognition signal distinct from the D box targeted by Cdh1. Genes Dev 14: 655-665.

Shakes, D. C., A. K. Allen, K. M. Albert and A. Golden, 2011 emb-1 encodes the APC16 subunit of the Caenorhabditis elegans anaphase-promoting complex. Genetics 189: 549-560.

Shimanovskaya, E., V. Viscardi, J. Lesigang, M. M. Lettman, R. Qiao et al., 2014 Structure of the C. elegans ZYG-1 cryptic polo box suggests a conserved mechanism for centriolar docking of Plk4 kinases. Structure 22: 1090-1104.

Song, M. H., L. Aravind, T. Muller-Reichert and K. F. O'Connell, 2008 The conserved protein SZY-20 opposes the Plk4-related kinase ZYG-1 to limit centrosome size. Dev Cell 15: 901-912.

Song, M. H., Y. Liu, D. E. Anderson, W. J. Jahng and K. F. O'Connell, 2011 Protein phosphatase 2A-SUR-6/B55 regulates centriole duplication in C. elegans by controlling the levels of centriole assembly factors. Dev Cell 20: 563-571.

Stubenvoll, M. D., J. C. Medley, M. Irwin and M. H. Song, 2016 ATX-2, the C. elegans Ortholog of Human Ataxin-2, Regulates Centrosome Size and Microtubule Dynamics. PLoS Genet 12: e1006370.

Strnad, P., S. Leidel, T. Vinogradova, U. Euteneuer, A. Khodjakov et al., 2007 Regulated HsSAS-6 levels ensure formation of a single procentriole per centriole during the centrosome duplication cycle. Dev Cell 13: 203-213.

Sugioka, K., D. R. Hamill, J. B. Lowry, M. E. McNeely, M. Enrick et al., 2017 Centriolar SAS-7 acts upstream of SPD-2 to regulate centriole assembly and pericentriolar material formation. Elife 6.

Tischer, T., J. Yang and D. Barford, 2022 The APC/C targets the Cep152-Cep63 complex at the centrosome to regulate mitotic spindle assembly. J Cell Sci 135.
Zhu, F., S. Lawo, A. Bird, D. Pinchev, A. Ralph et al., 2008 The mammalian SPD-2 ortholog Cep192 regulates centrosome biogenesis. Curr Biol 18: 136-141.

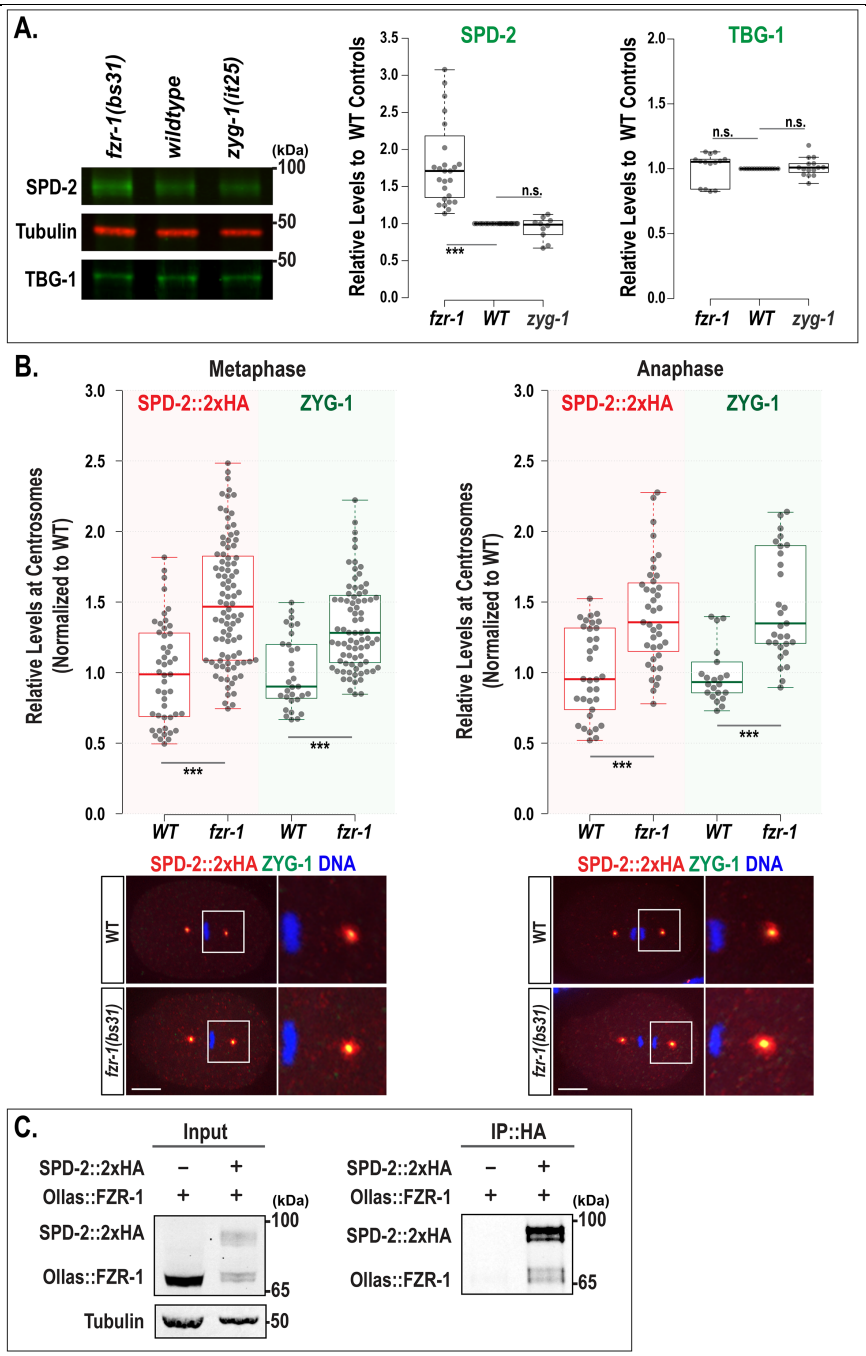

Figure 1. Loss of FZR-1 stabilizes SPD-2. (**A**) Representative western blot with anti-SPD-2 and anti-TBG-1 using embryonic lysates from *fzr-1(bs31)* mutants, wild-type(*N2*), and *zyg-1(it25)* mutants (Left). Tubulin was used as a loading control. Quantitative western blot analysis shows significantly increased levels of SPD-2 (Middle) in *fzr-1(bs31)* mutants (1.89±0.71-fold, $p<0.001$, n=27), but no change in *zyg-1(it25)* mutants (0.94±0.16-fold, $p=0.49$, n=10), compared to wild-type (WT) controls (1.00±0.0-fold, n=24). In contrast, there were no significant differences in TBG-1 levels (Right) among *fzr-1(bs31)* mutants (1.01±0.12-fold, $p=0.80$, n=14), *zyg-1(it25)* mutants (1.01±0.07-fold, $p=0.53$, n=15), and wild-type controls (1.00±0.0-fold, n=15). (**B**) (Top) Quantification of total centrosomal SPD-2::2xHA and ZYG-1 levels during the first mitotic cycle. Each dot represents a centrosome. (Bottom) Embryos stained for SPD-2::2xHA and ZYG-1 at the first mitotic metaphase and anaphase, with magnified images of posterior centrosomes. Bar, 10 μm. In the plots, the box ranges from the first through the third quartile of the data. The thick bar indicates the median. The solid grey line extends 1.5 times the inter-quartile range or to the minimum and maximum data points. $^{ns}p>0.05$, $^{***}p<0.001$ (two-tailed t-tests). (**C**) IP using anti-HA suggests that SPD-2 physically interacts with FZR-1. Embryonic extracts from Ollas::FZR-1 expressing embryos were used as a negative control; ~1% of the total lysates were loaded in the input lanes.

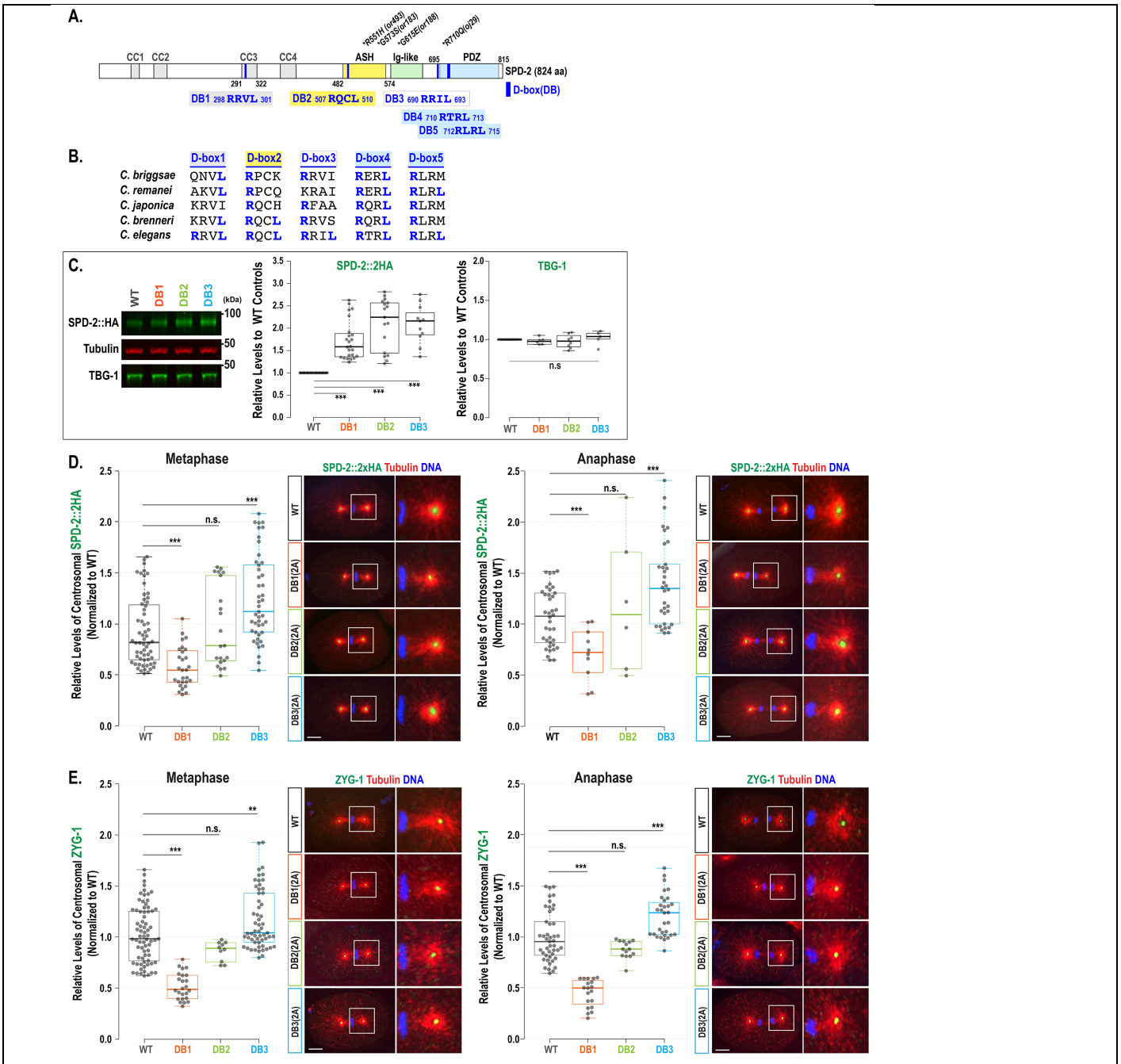

Figure 2. Mutating D-box motifs elevates overall SPD-2 levels. (**A**) SPD-2 protein structure illustrates the locations of D-boxes (DB1 through 5), functional domains, and mutant alleles. (**B**) Sequence alignments of D-box motifs (1 through 5) in the *Caenorhabditis* species. (**C**) (Left) Representative western blot with anti-HA and anti-TBG-1 using embryonic lysates from individual degron mutants, wild-type (WT) controls expressing 2xHA. Tubulin was used as a loading control. (Middle) Quantitative western blot analysis shows significantly increased levels of SPD-2::2xHA in all three degron mutants. (Right) In contrast, there were no significant differences in TBG-1 levels among *fzr-1(bs31)* mutants (1.01±0.12-fold, p=0.80, n=14), *zyg-1(it25)* mutants (1.01±0.07-fold, p=0.53, n=15), degron mutants and wild-type controls (1.00±0.0-fold, n=15). (**D-E**) (Left) Quantification of total centrosomal SPD-2::2xHA levels during the first mitotic cycle. Each dot represents a centrosome. (Right) Embryos stained for (**D**) SPD-2::2xHA and (**E**) ZYG-1 at the first mitotic metaphase and anaphase, with magnified images of posterior centrosomes. Bar, 10 μm. (**C-E**) In the plots, the box ranges from the first through the third quartile of the data. The thick bar indicates the median. The solid grey line extends 1.5 times the inter-quartile range or to the minimum and maximum data points. ^{ns}p>0.05, $^{**}p$<0.01, $^{***}p$<0.001 (two-tailed t-tests).

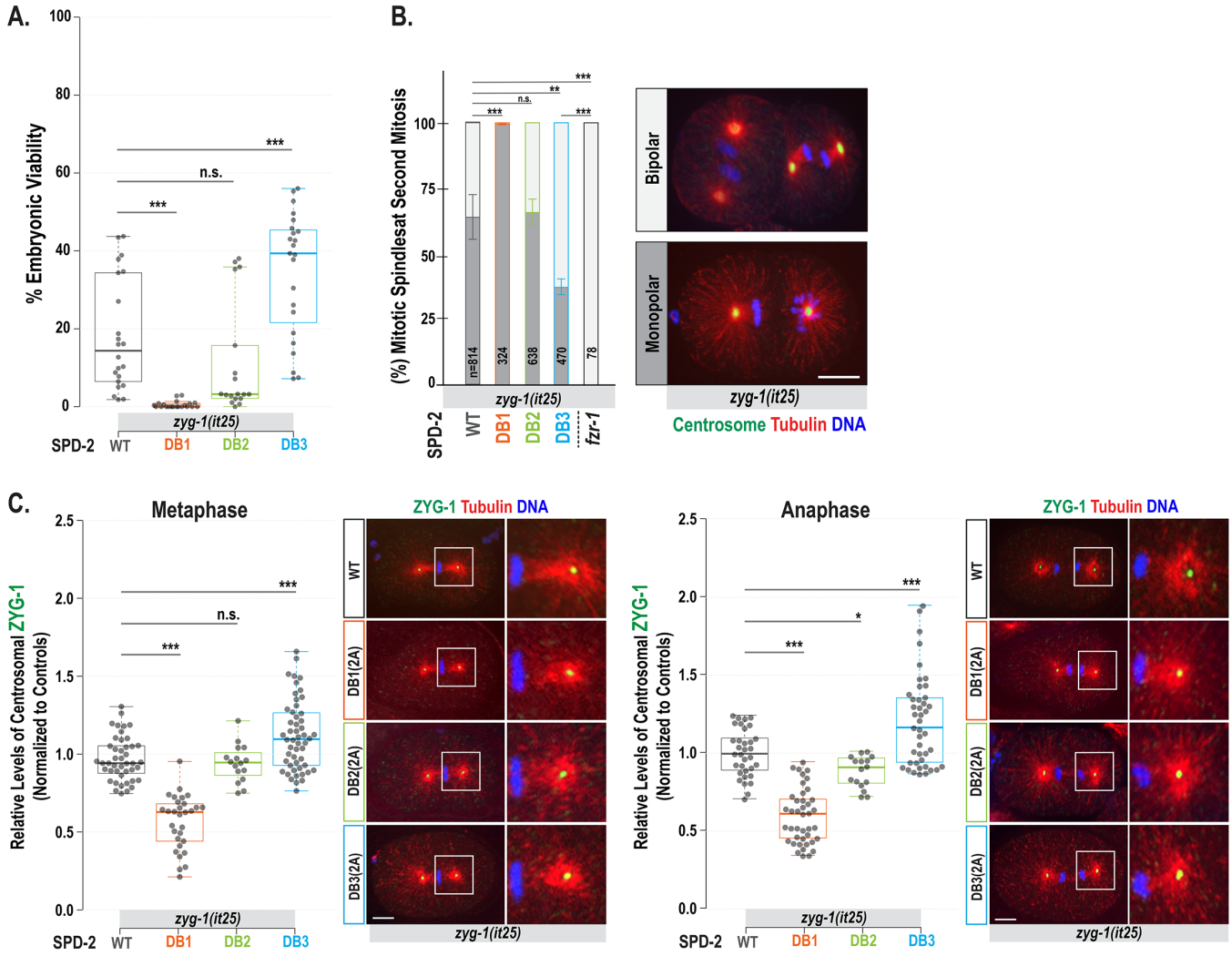

Figure 3. Mutating SPD-2 D-box3 leads to the *zyg-1* suppression and elevated centrosomal ZYG-1 levels. (**A**) Embryonic viability at 22.5°C (See Table 1). Each dot represents a hermaphrodite. (**B**) Quantification of monopolar (dark grey) and bipolar (light grey) spindles in two-cell embryos at 23°C. Average and standard deviation (SD) are presented. n is the number of blastomeres (left). Embryos stained for centrosomes (SAS-4), microtubules and DNA, illustrate mitotic spindles at second division. (**C**) (Left) Quantification of centrosome-associated ZYG-1 levels at the first mitotic metaphase and anaphase in *zyg-1(it25)* mutant backgrounds. Each dot represents a centrosome. (Right) Centrosomes stained for ZYG-1 during the first mitotic cycle, with magnified images of posterior centrosomes. (**B-C**) Bar, 10 μm. (**A,C**) In the plots, box ranges from the first through third quartile of the data. Thick bar indicates the median. Solid grey line extends 1.5 times the inter-quartile range or to the minimum and maximum data point. $^{ns}p>0.05$, $^{**}p<0.01$, $^{***}p<0.001$ (two-tailed t-tests).

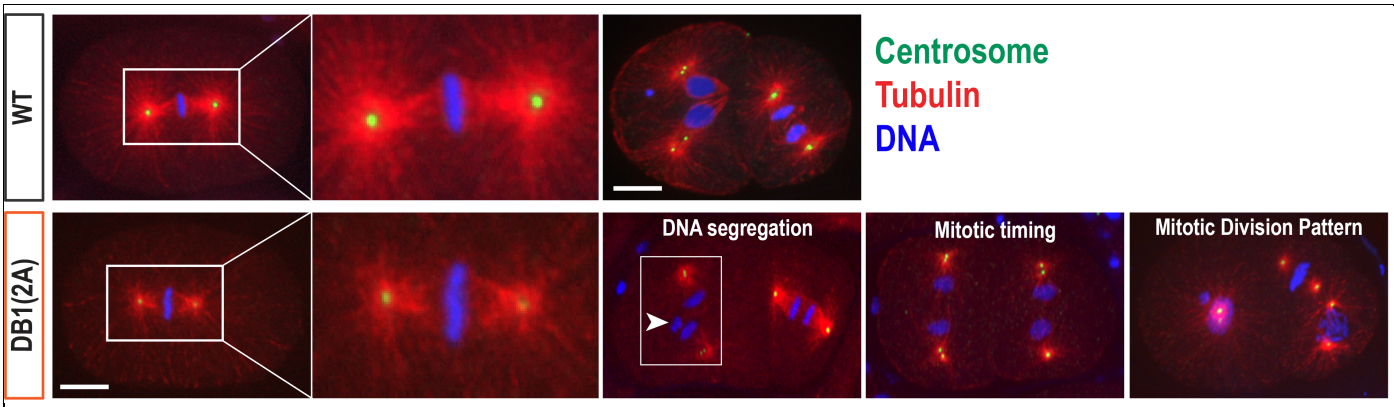

Figure 4. SPD-2:DB1(2A) mutant embryos exhibit abnormal cell division phenotypes. SPD-2:DB1(2A):2xHA mutant embryos stained for centrosomes (SAS-4), microtubules, and DNA. At 25°C, DB1(2A) mutant embryos display abnormal cell division phenotypes, including tiny centrosomes and often highly asymmetric centrosome sizes during the first mitotic metaphase, as well as abnormal patterns in DNA segregation, cell division timing, and mitotic division compared to the WT control. Arrowhead indicates ectopic DNA. Bar, 10 μm.